Research article

NMR IN BIOMEDICINE

Received: 1 October 2013, Revised: 6 May 2014, Accepted: 23 May 2014, Published online in Wiley Online Library: 7 July 2014

(wileyonlinelibrary.com) DOI: 10.1002/nbm.3153

Glioma grading using apparent diffusion coefficient map: application of histogram analysis based on automatic segmentation

Jeongwon Lee[a,b], Seung Hong Choi[c], Ji-Hoon Kim[c], Chul-Ho Sohn[c], Sooyeul Lee[b] and Jaeseung Jeong[a]***

The accurate diagnosis of glioma subtypes is critical for appropriate treatment, but conventional histopathologic diagnosis often exhibits significant intra-observer variability and sampling error. The aim of this study was to investigate whether histogram analysis using an automatically segmented region of interest (ROI), excluding cystic or necrotic portions, could improve the differentiation between low-grade and high-grade gliomas. Thirty-two patients (nine low-grade and 23 high-grade gliomas) were included in this retrospective investigation. The outer boundaries of the entire tumors were manually drawn in each section of the contrast-enhanced T_1-weighted MR images. We excluded cystic or necrotic portions from the entire tumor volume. The histogram analyses were performed within the ROI on normalized apparent diffusion coefficient (ADC) maps. To evaluate the contribution of the proposed method to glioma grading, we compared the area under the receiver operating characteristic (ROC) curves. We found that an ROI excluding cystic or necrotic portions was more useful for glioma grading than was an entire tumor ROI. In the case of the fifth percentile values of the normalized ADC histogram, the area under the ROC curve for the tumor ROIs excluding cystic or necrotic portions was significantly higher than that for the entire tumor ROIs ($p < 0.005$). The automatic segmentation of a cystic or necrotic area probably improves the ability to differentiate between high- and low-grade gliomas on an ADC map. Copyright © 2014 John Wiley & Sons, Ltd.

Keywords: glioma; grade; diffusion-weighted MRI; apparent diffusion coefficient maps

INTRODUCTION

Gliomas are the most common type of primary brain tumor in adults and a critical cause of cancer mortality. According to the World Health Organization (WHO), gliomas can be classified into four grades, which are determined by the pathologic evaluation of the tumor. Low-grade gliomas (grades I and II) are well differentiated and not benign, but still portend a better prognosis for the patient. In contrast, high-grade gliomas (grades III and IV) are undifferentiated and malignant, and carry a worse prognosis (1). An accurate classification between low-grade and high-grade gliomas is particularly significant for the planning of treatment strategies and for predicting treatment response and prognosis. The current gold standards for grading are standard tumor morphologic observations and histopathologic diagnosis, but these methods have limitations of significant intra-observer variability and sampling error (2,3).

Recently, several imaging methods and automatic classification methods have been proposed and investigated. These use information from the entire tumor to determine the glioma grade. Diffusion-weighted MRI is one of the most promising methods for the characterization of brain tumors. Several studies have reported that apparent diffusion coefficient (ADC) maps, which indicate the magnitude of the diffusion of water molecules within cerebral tissue obtained from several diffusion-weighted images, may be useful for preoperative grading (3,4). However, the role of ADC maps in differentiating between low-grade and high-grade gliomas has been disputed (5,6). A number of studies have shown that reduced ADC values can be clearly detected in high-grade gliomas (7–12). However, others have reported that it is not possible to differentiate between high-grade and low-grade gliomas using ADC maps alone (13–15).

The sampling error of the regions of interest (ROIs), as a result of tissue heterogeneity, has been suggested to be an important reason for this discrepancy in the applicability of ADC maps to

* *Correspondence to: J. Jeong, Department of Bio and Brain Engineering, Korea Advanced Institute of Science and Technology (KAIST), 294 Daehak-Ro, Daejeon 305-701, South Korea.*
E-mail: jsjeong@kaist.ac.kr
** *Correspondence to: S. H. Choi, Department of Radiology, Seoul National University College of Medicine, 28, Yongon-dong, Jongno-gu, Seoul 110-744, South Korea.*
E-mail: verocay@snuh.org

a *J. Lee, J. Jeong*
Department of Bio and Brain Engineering, Korea Advanced Institute of Science and Technology (KAIST), Daejeon, South Korea

b *J. Lee, S. Lee*
Medical Imaging Research Section, Electronics and Telecommunications Research Institute (ETRI), Daejeon, South Korea

c *S. H. Choi, J.-H. Kim, C.-H. Sohn*
Department of Radiology, Seoul National University College of Medicine, Seoul, South Korea

Abbreviations used: *ADC, apparent diffusion coefficient; AUC, area under the curve; CSF, cerebrospinal fluid; FLAIR, fluid attenuated inversion recovery; NADC, normalized apparent diffusion coefficient; PACS, picture archiving and communication system; ROC, receiver operating characteristic; ROI, region of interest; WHO, World Health Organization.*

differentiate between tumor grades (9,16). A number of previous studies (8,10,17) have used several small-sample ROIs. The ROIs were manually placed within solid tumor components on each section of the T_1 images or ADC maps. They were carefully placed to avoid cystic or necrotic areas because these areas contribute to an increase in the ADC values. The ROIs were usually round or oval in shape, and their areas ranged from 10 pixels (10,17) to more than 20 pixels (8). Therefore, analysis with small-sample ROIs may not avoid sampling error; it may not reflect the characteristics of the entire tumor.

To avoid the problem of ROI sampling error, a histogram analysis using an entire tumor ROI has been employed on ADC maps. A previous study (18) used the entire tumor volume, which was manually drawn on the ADC maps, in order to allow the use of all ADC values within the tumor. In addition, a recent study (4) performed a histogram analysis using the entire tumor ROI on ADC maps; its results demonstrated that the fifth percentile of the cumulative ADC histogram was the most promising parameter for differentiating between high-grade and low-grade gliomas. However, the use of the entire tumor ROI has a disadvantage over the use of small-sample ROIs in that the entire tumor ROI also includes cystic or necrotic areas, which thus lead to increased ADC values.

Here, we propose to analyze the ADC values of the tumor ROI excluding cystic or necrotic portions. Our hypothesis is that a tumor ROI excluding cystic or necrotic portions will show a higher correlation with the tumor characteristics than will an entire tumor ROI. Necrotic areas, which appear more commonly in high-grade gliomas than in low-grade gliomas, present high ADC values, as do cystic areas. These high ADC values may negatively affect the ability to differentiate between low-grade and high-grade gliomas, because our baseline assumption is that high-grade gliomas present low ADC values.

Therefore, the aim of this study was to investigate whether histogram analysis within a tumor ROI excluding cystic or necrotic portions improves the differentiation between low-grade and high-grade gliomas. To test our hypothesis, we investigated the MR images of 32 patients (nine low-grade gliomas and 23 high-grade gliomas) and performed analyses on ADC values within the manually drawn entire tumor volume and within the tumor ROIs excluding cystic or necrotic portions; we then compared the ROC curves of differentiation for the low-grade and high-grade gliomas. We expected that a tumor ROI excluding necrotic or cystic areas would be more able to differentiate between low-grade and high-grade gliomas than would an entire tumor ROI.

MATERIALS AND METHODS

Subjects

Initially, 54 patients underwent MRI at Seoul National University Hospital between December 2006 and October 2011. Patients with previous treatment or other concurrent brain diseases were excluded from this study. In addition, one patient was excluded as an outlier using Tukey's method (19). Thus, 32 patients (nine men and 23 women; mean age, 48 years; range, 22–76 years) with primary cerebral gliomas (nine low-grade gliomas and 23 high-grade gliomas) were finally included in this study: WHO grade I astrocytomas ($n = 2$), grade II astrocytomas ($n = 7$), grade III astrocytomas ($n = 5$) and grade IV glioblastomas ($n = 18$). The WHO grades of all the patients were proven by histopathologic assessment.

MRI

Twenty-one cases were acquired using a 1.5-T MR scanner (Signa Excite or Signa HDxt, GE Medical Systems, Milwaukee, WI, USA) and 11 were obtained using a 3-T MR imager (Magnetom Verio, Siemens Medical Systems, Erlangen, Germany) with an eight-channel head coil. In the 1.5-T images, T_1-weighted axial images were obtained with TR/TE of 500/8 or 666/20 ms, 30 sections, a section thickness of 5 mm, a matrix of 512×512 pixels and a voxel resolution of $0.43 \times 0.43 \times 5.0\ mm^3$. T_2-weighted fast-spin-echo images were acquired with TR/TE of 3050/100 or 5000/128 ms, 25 sections, a section thickness of 5 mm, an intersection gap of 6 mm, a matrix of 512×512, an echo train length of 16 and a voxel resolution of $0.43 \times 0.43 \times 5.0\ mm^3$. Echo-planar diffusion-weighted images were acquired in the axial plane before the injection of contrast material with TR/TE of 6500/70 or 10 000/65 ms (at $b = 0$ and $1000\ s/mm^2$), 25 sections, a bandwidth of 1953 Hz/voxel, a section thickness of 3 or 5 mm, an intersection gap of 4 or 6 mm, a matrix of 256×256, two acquired signals and a pixel resolution of 0.94×0.94. However, in the 3-T images, T_1-weighted axial images were obtained with TR/TE of 1500/1.9 or 742/9.8 ms, 160 sections, a section thickness of 1 mm, a matrix of 256×256 pixels and a voxel resolution of $0.57 \times 0.57 \times 1$ or $0.97 \times 0.97 \times 1$ mm. T_2-weighted fast-spin-echo images were acquired with TR/TE of 5160/91 ms, 25 sections, a section thickness of 5 mm, an intersection gap of 6 mm, a matrix of 580×640, an echo train length of 16 and a voxel resolution of $0.34 \times 0.34 \times 5.0\ mm^3$. Echo-planar diffusion-weighted images were acquired in the axial plane before the injection of contrast material with TR/TE of 6900/55 ms (at $b = 0$ and $1000\ s/mm^2$), 25 sections, a bandwidth of 1202 Hz/voxel, a section thickness of 3 mm, an intersection gap of 3.9 mm, a matrix of 320×320, two acquired signals and a voxel resolution of $0.75 \times 0.75 \times 3.0\ mm^3$. In addition, diffusion-weighted images were acquired in three orthogonal directions and combined into a trace image. ADC maps were calculated on a voxel-by-voxel basis with the built-in software of the MRI units. In all 32 patients, axial T_1-weighted images were obtained after the intravenous administration of a single dose of gadopentetate dimeglumine (Magnevist; Bayer Pharma AG, Berlin, Germany) with a fat suppression pulse.

Image analysis

The images of the patients were evaluated retrospectively. All the images were transferred from the picture archiving and communication system (PACS) workstation to a personal computer and converted to NIfTI format, which is used in SPM8, employing the free software dcm2nii in MRIcron. The T_2-weighted images, together with the ADC maps at $b = 1000\ s/mm^2$, were co-registered with the T_1-weighted images using a normalized mutual information algorithm in statistical parametric mapping (SPM8; University College London, London, UK) (20). T_2-weighted MR images and ADC maps were re-sliced into a 256×256 matrix of T_1-weighted MR images. The within-subject registration was processed using a three-dimensional rigid-body transformation (21) employing trilinear interpolation.

The boundaries of the entire tumors were manually drawn in each section of the contrast-enhanced T_1-weighted MR images by a radiologist (see Fig. 1a). When there was no enhancement of the contrast-enhanced T_1-weighted MR images, the areas with

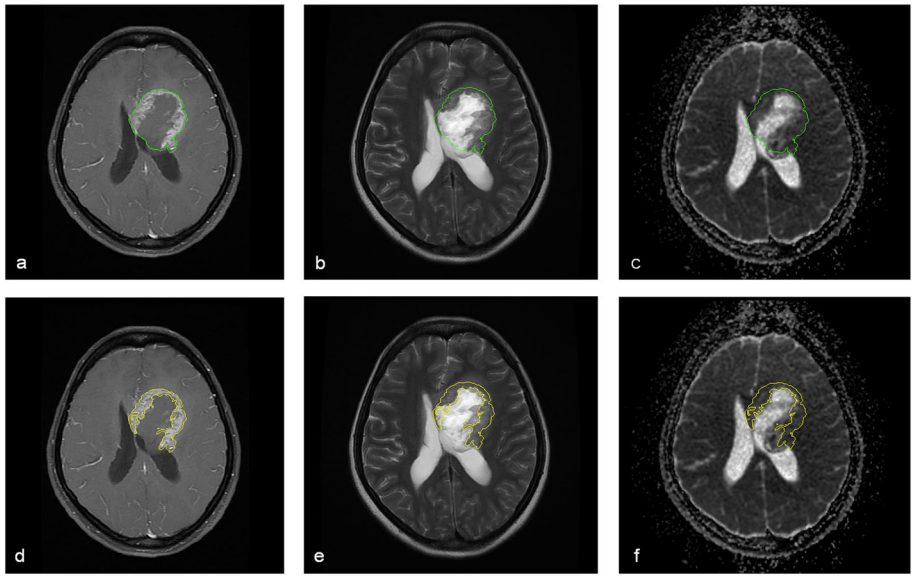

Figure 1. High-grade glioma. (a) Axial post-contrast T_1-weighted image. (b) Axial T_2-weighted image. (c) Apparent diffusion coefficient (ADC) map. The boundary of the entire tumor was manually drawn on the T_1-weighted image. The boundaries of the entire tumor volume (green line) were copied to the T_2-weighted image and ADC map. T_2-weighted image and ADC map were co-registered with T_1-weighted image. (d) The same slice as in (a). (e) The same slice as in (b). (f) The same slice as in (c). The tumor lesion excluding cystic or necrotic areas (yellow line) was automatically segmented.

high intensity were drawn on T_2-weighted MR images or FLAIR (fluid attenuated inversion recovery) images. Manual segmentation was performed on the in-house software developed with Microsoft Visual C++ (version 2008; Microsoft, Redmond, WA, USA). The boundaries of entire tumors were loaded onto the ADC maps at $b = 1000$ s/mm^2 (Fig. 1b, c).

In order to obtain the tumor ROIs excluding cystic or necrotic portions, we assumed that the cystic or necrotic portions met two conditions: first, no enhancement with contrast agent in the T_1-weighted images and, second, high intensity, like cerebrospinal fluid (CSF), in the T_2-weighted images. We implemented the automatic segmentation algorithm using the Otsu threshold method (22) in the T_1-weighted images for the first condition (Fig. 1d). For the second condition, we placed an ROI within a normal-appearing CSF region in the T_2-weighted images; we used the minimum value in the ROI as a threshold to segment a cystic or necrotic portion (Fig. 1e). A tumor lesion excluding cystic or necrotic portions was finally obtained using extraction of the intersection of the candidates obtained using the two conditions (Fig. 1f). The histogram of the tumor ROIs excluding cystic or necrotic portions had a lower relative frequency at high ADC values (Fig. 2). This difference between the histograms of the two ROIs implies that the automatically segmented area may correspond to the cystic or necrotic area, because cystic or necrotic areas represent high intensity on ADC maps.

Before the analysis of the ADC values, to minimize the variability in the absolute ADC values between the different diffusion-weighted MRI sequences and the different hardware configurations, normalized ADC (NADC) ratios were obtained from the respective ADC values within the ROIs (23–25). NADC ratios were calculated using the formula, NADC = ADC value of the ROIs/ADC value of normal white matter (26–28). The ADC value of normal white matter on an ADC map was obtained from the average of three square ROIs of different sections. The ROIs were manually placed within contralateral normal-appearing white matter (26–28) (Fig. 3).

To analyze the characteristics of the tumors, various parameters were obtained from the NADC ratios within the ROIs; the first, fifth and tenth percentile points (C_1, C_5 and C_{10}, respectively) of the cumulative NADC histogram and the mean NADC. The analysis was performed automatically with an in-house software program developed using MATLAB (MathWorks Inc., Natick, MA, USA).

Statistical analysis

All statistical analyses were performed with a statistical package (MedCalc, version 11.1.1.0; MedCalc Software, Mariakerke, Belgium). The normality of the parameters was assessed with the Kolmogorov and Smirnov tests. To compare the parameters between high-grade and low-grade gliomas, a two-tailed unpaired Student's *t*-test was applied. To assess whether a tumor ROI excluding cystic or necrotic portions provided better performance in the differentiation between low-grade and high-grade gliomas than did an entire tumor ROI, receiver operating characteristic (ROC) curves were calculated and the area under the curve (AUC) results were compared using the method of Hanley and McNeil (29). Results were validated using a leave-one-out cross-validation (30). In each round of the leave-one-out validation, one patient was selected as a testing sample; the remaining participants were used as training samples. The results with p values of less than 0.05 were considered to be statistically significant.

RESULTS

First, we validated the normalization of the ADC values using contralateral normal-appearing white matter. There were no statistically significant differences between the 1.5-T data and the 3-T data when considering the mean ADC value of the contralateral normal-appearing white matter ($p > 0.05$). Moreover, there were no significant differences between the low-grade and high-grade gliomas with regard to the mean ADC value of the contralateral normal-appearing white matter ($p > 0.05$).

NMR IN BIOMEDICINE

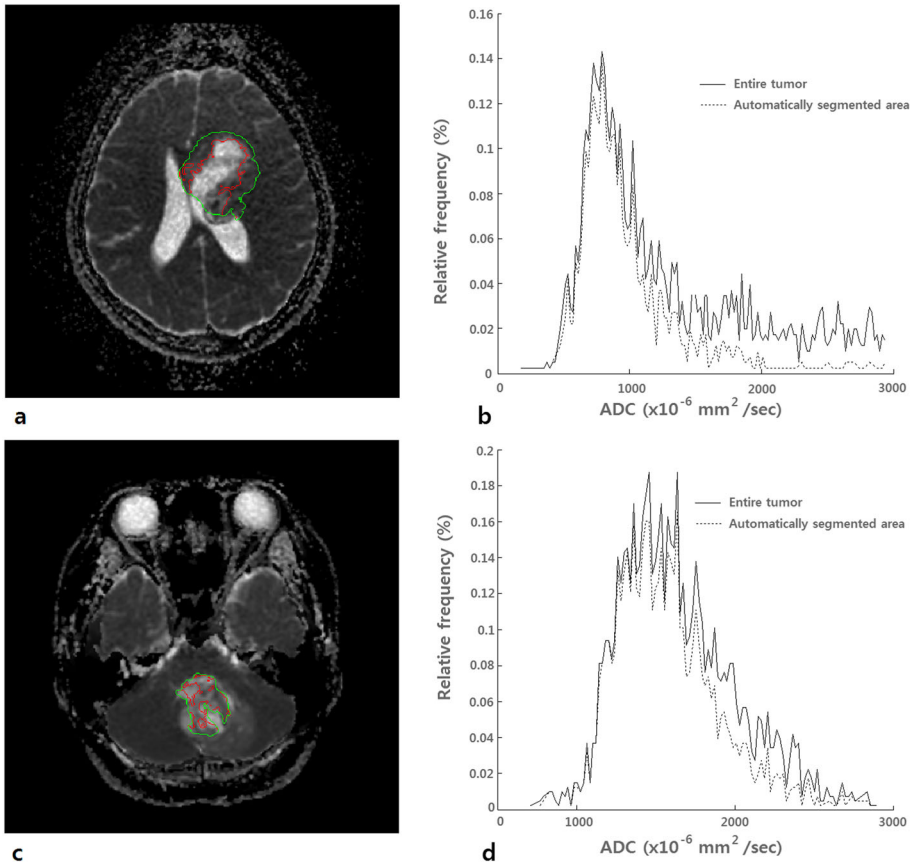

Figure 2. Apparent diffusion coefficient (ADC) map and histogram. (a) ADC map of a high-grade glioma from Fig. 1. (b) ADC histogram of two regions of interest (ROIs) in (a). (c) ADC map of a low-grade glioma. (d) ADC histogram of two ROIs in (c). In ADC maps, the green line represents the entire tumor area and the red line represents the automatically segmented area. In ADC histograms, the full line represents the histogram within the entire tumor area and the broken line represents the histogram within the automatically segmented area. Automatically segmented areas were obtained by the extraction of cystic and necrotic areas from the entire tumor volume. The histogram of the automatically segmented area demonstrates reduced relative frequency in the high-ADC portion, because cystic and necrotic areas have high intensity on ADC maps.

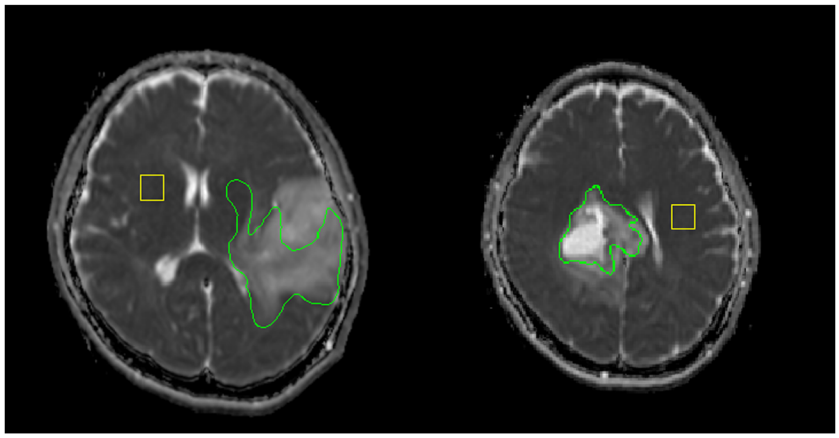

Figure 3. Apparent diffusion coefficient (ADC) map: (a) low-grade glioma; (b) high-grade glioma. The boundaries of the entire tumor volume (green line) were copied to the ADC map. A region of interest (ROI) for normalization of the ADC value (yellow rectangle) was placed within the contralateral normal-appearing white matter.

We compared the mean values of each parameter within the tumor ROIs excluding cystic or necrotic portions and the entire tumor ROIs in both low-grade and high-grade gliomas (Table 1). We found that the parameters of the NADC ratios of high-grade gliomas were lower than those of low-grade gliomas, as expected. Furthermore, the NADC values were lower in the tumor ROI excluding cystic or necrotic portions than in the entire tumor ROIs, as expected.

A major finding was that the area under the ROC curve for the 5th percentile of the tumor ROIs excluding cystic or necrotic portions was 0.754, which was significantly better than the performance for the entire tumor ROIs of 0.720 ($p < 0.005$) (Figs. 4 and 5).

Table 1. Histogram parameters for low- and high-grade gliomas

Parameter	ROI	LGGs	HGGs	AUC	*p*
C_1	Entire tumor	1.08 ± 0.20	0.91 ± 0.23	0.754	0.0033
	Automatically segmented area	1.07 ± 0.20	0.89 ± 0.22	0.763	0.0018
C_5	Entire tumor	1.25 ± 0.28	1.05 ± 0.25	0.720	0.0192
	Automatically segmented area	1.24 ± 0.27	1.03 ± 0.23	0.754	0.0043
C_{10}	Entire tumor	1.35 ± 0.33	1.13 ± 0.26	0.691	0.0501
	Automatically segmented area	1.34 ± 0.34	1.10 ± 0.24	0.720	0.0205
$NADC_{mean}$	Entire tumor	1.78 ± 0.46	1.73 ± 0.47	0.546	0.6816
	Automatically segmented area	1.74 ± 0.43	1.55 ± 0.32	0.628	0.2301

ADC, apparent diffusion coefficient; AUC, area under the receiver operating characteristic (ROC) curve; C_1, C_5 and C_{10}, first, fifth and tenth percentile points of the cumulative normalized ADC histogram, respectively; HGGs, high-grade gliomas; LGGs, low-grade gliomas; $NADC_{mean}$, mean value of the normalized ADC ratios; ROI, region of interest.
Values are the mean of each parameter and are expressed as the mean ± standard deviation.

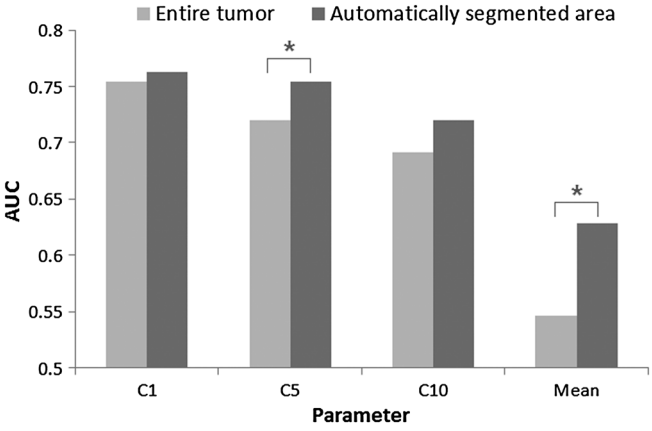

Figure 4. Area under the receiver operating characteristic (ROC) curves (AUC) in terms of histogram parameters and regions of interest (ROIs). C_1, C_5 and C_{10} are the first, fifth and tenth percentile points of the cumulative normalized ADC (NADC) histogram, respectively. There were significant differences between the two ROIs for C_5 and mean NADC ($p < 0.05$).

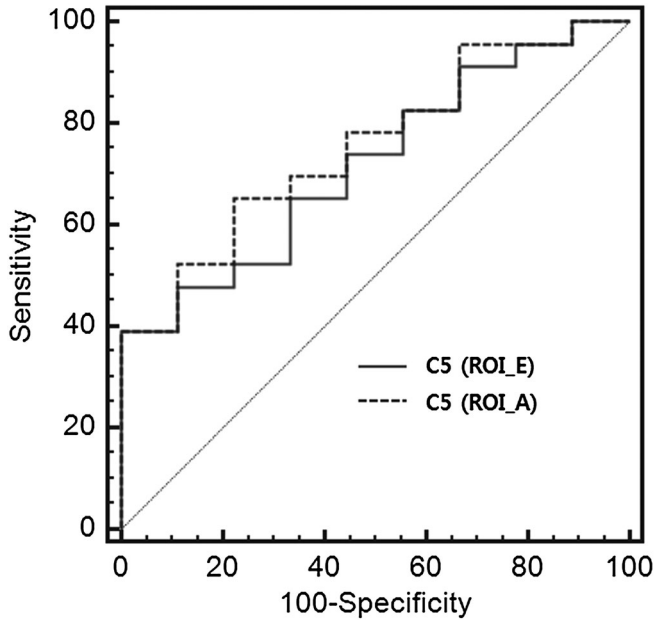

Figure 5. Receiver operating characteristic (ROC) curves for different regions of interest (ROIs). The full line represents the fifth percentile (C_5) in the entire tumor ROI (ROI_E); the broken line represents the fifth percentile (C_5) in the automatically segmented area (ROI_A).

This result suggests that the proposed method of ROI selection may improve the histogram analysis of ADC values for glioma grading. For the mean NADC, there was also a significant difference between the two ROIs; however, the mean NADC was not a significant parameter that could be used to differentiate between low-grade and high-grade gliomas ($p > 0.05$) (Table 1).

DISCUSSION

This study was designed to assess whether the exclusion of cystic or necrotic portions from a tumor ROI improves the differentiation between low-grade and high-grade gliomas. The results obtained from this study suggest that our proposed analysis of ADC maps based on the segmentation of cystic or necrotic areas is a potentially useful method for differentiating between low-grade and high-grade gliomas.

Several previous studies (7–12) have demonstrated that histogram analysis of ADC values within tumor lesions is potentially useful for the grading of gliomas, whereas other studies have reported that it is not possible to differentiate between high-grade and low-grade gliomas using diffusion-weighted imaging and ADC values alone (13–15). The sampling bias of ROIs as a result of tissue heterogeneity has been cited as a possible reason for the conflicting results on the usefulness of ADC values in tumor grading (9,16). In most of the previous studies, several ROIs were placed manually within solid tumor components in each section of the T_1 images or ADC maps to calculate the parameters related to ADC values. Yet, the small-sample ROI selection methods in the previous studies were quite limited in their application to the analysis of ADC for brain tumors. When entire tumor ROIs are not investigated during image analysis, the average ADC value might not correspond to the true mean ADC of the entire tumor lesion (18). Furthermore, using small-sample ROIs, the localized area within a tumor can be subjective and prone to sampling bias. Kang *et al.* (4) have argued that this sampling bias accounts for the discrepancies among the results of previous studies (18,31,32) on the usefulness of diffusion-weighted MRI in

distinguishing between high- and low-grade gliomas. Thus, an entire tumor ROI probably represents the characteristics of a tumor more accurately than do several ROI samples in a tumor lesion on ADC maps.

However, in previous studies using small-sample ROIs (8,22,18,33–35), the ROIs were carefully placed in order to avoid cystic or necrotic areas that would influence the ADC values, because cystic or necrotic areas are more frequent in high-grade gliomas and consequently increase ADC values (34). Necrosis is a type of cell death caused by tumor hypoxia as a result of increased cell proliferation and mitotic activity (36). Necrosis may appear like cysts in conventional and diffusion-weighted MRI. In gadolinium contrast T_1-weighted images, necrotic areas are not enhanced. In T_2-weighted images, necrotic areas have high intensity, like CSF. Areas of necrotic lesions have low intensity in diffusion-weighted MR images and high intensity in ADC maps, because necrosis equates to low cellularity. In ADC maps, active tumor lesions may have low intensity and necrotic areas may have high intensity. A previous study (37) reported a high correlation between the degree of tumor necrosis at pathology and the ADC values of ROIs. Accordingly, the mean ADC values in entire tumor lesions including cystic or necrotic areas are higher than those in active tumor lesions. Necrosis often occupies a large portion of a tumor lesion. Thus, we speculate that necrosis is possibly a confusing factor for the grading of gliomas based on ADC maps. Some of the conflicting results from various studies on the differentiation between low-grade and high-grade gliomas potentially may be influenced by how carefully the ROIs exclude cystic or necrotic portions for the analyses of ADC values. For this reason, we assumed that tumor lesions excluding cystic or necrotic areas present the characteristics of tumor cells; thus, in this study, we attempted to extract cystic or necrotic portions from the entire tumor lesions.

Our hypothesis was that the exclusion of cystic or necrotic portions from the entire tumor ROI may improve the differentiation between low-grade and high-grade gliomas. Accordingly, we compared the area under the ROC curve for tumor ROIs excluding cystic or necrotic portions with that for entire tumor ROIs. We found that the area under the ROC curve for the 5th percentile with an automatically segmented area was 0.754, which was significantly better than the performance of the entire tumor ROIs, which was 0.720 in our data ($p < 0.005$). Therefore, our results suggest that the automatically segmented ROI excluding cystic or necrotic portions probably improves the ability to differentiate between high-grade and low-grade gliomas.

There was no significant difference between the AUC for C_1 and C_5 ($p > 0.05$), although C_1 showed a larger AUC than that of C_5. According to a previous study (4), C_5 is potentially the most promising parameter for the differentiation between high-grade and low-grade gliomas. We speculate that a C_5 value obtained from a cumulative NADC histogram can be presumed to be less affected by misregistration artifacts or extreme NADC values resulting from diffusion-weighted MRI (4). In addition, our findings for this study suggest that an automatically segmented ROI excluding cystic or necrotic portions from an entire tumor strongly improves the differentiation between low-grade and high-grade gliomas when using the C_5 parameter of the cumulative NADC histogram.

The limitations of this study must be acknowledged. The first limitation is the use of data obtained from 1.5-T and 3-T MR scanners. No studies have yet been performed to assess the influence of field strength on ADC values in head and neck cancers. However, Chawla *et al.* (38) reviewed previous reports and suggested that ADC is a field strength-independent parameter; their results allowed us to compare results across different sites and different field strengths. Kim *et al.* (39) reported that there was no difference in the ADC values from the submandibular glands of three healthy human subjects when measured using 1.5-T and 3-T scanners. In addition, Donati *et al.* (40) reported that ADC values of the gallbladder, pancreas, spleen and kidney were comparable among MR systems from different vendors and among different field strengths. Furthermore, we used NADC ratios to minimize the differences in ADC values caused by different levels of magnetic fields and to eliminate inter-image variability (25). Therefore, we combined the images from the 1.5-T and 3-T scanners to supplement the limitation of the small amount of data; however, the lack of patient data still remains a limitation.

The second limitation of this study was the sample size discrepancy between low- and high-grade gliomas. However, this discrepancy is a result of clinical incidence rather than data selection. Low-grade gliomas show lower incidence than high-grade gliomas in consecutive adult patients.

The third limitation of this study was that the ADC values were calculated by monoexponential fitting. Currently, for most commercial MRI systems, the ADC value is calculated automatically and, by default, using a monoexponential function and all available b value images (41). However, simple monoexponential fitting between an MR signal and a b value may not fully account for tissue behavior. Therefore, biexponential fitting (42–44) or stretched exponential fitting (45) have been investigated for intravoxel incoherent motion analysis. However, we do not argue that we have segmented the cystic or necrotic regions exactly. Even if the ADC maps were calculated using a multi-exponential function, we can expect that the automatically segmented areas would improve the diagnostic accuracy.

Acknowledgements

This work was supported by the research collaboration program of the Korea Research Council for Industrial Science and Technology [Development of convergent radiotherapy equipment with O-arm CT] (JL and SL) and the Korea Science and Engineering Foundation (KOSEF) grant funded by the Korean Government (MOST) (No. R01-2007-000-21094-0, NRF-2006-2005399, and No. M10644000028-06 N4400-02810) (JJ), and the grant funded by National IT Industry Promotion Agency (NIPA) (H0502-13-1086) (JJ).

REFERENCES

1. Stupp R, Tonn J-C, Brada M, Pentheroudakis G. High-grade malignant glioma: ESMO Clinical Practice Guidelines for diagnosis, treatment and follow-up. Ann. Oncol. 2010; (21 Suppl.)5: v190–v193.
2. Law M, Oh S, Babb JS, Wang E, Inglese M, Zagzag D, Knopp EA, Johnson G. Low-grade gliomas: dynamic susceptibility-weighted contrast-enhanced perfusion MR imaging—prediction of patient clinical response. Radiology 2006; 238: 658.
3. Arvinda HR, Kesavadas C, Sarma PS, Thomas B, Radhakrishnan VV, Gupta AK, Kapilamoorthy TR, Nair S. Glioma grading: sensitivity, specificity, positive and negative predictive values of diffusion and perfusion imaging. J. Neuro-Oncol. 2009; 94: 87–96.
4. Kang Y, Choi SH, Kim YJ, Kim KG, Sohn CH, Kim JH, Yun TJ, Chang KH. Gliomas: histogram analysis of apparent diffusion coefficient maps with standard- or high-b-value diffusion-weighted MR imaging—correlation with tumor grade. Radiology 2011; 261(3): 882–890.

5. Waldman AD, Jackson A, Price SJ, Clark CA, Booth TC, Auer DP, Tofts PS, Collins DJ, Leach MO, Rees JH. Quantitative imaging biomarkers in neuro-oncology. Nat. Rev. Clin. Oncol. 2009; 6: 445–454.
6. Scarabino T, Popolizio T, Trojsi F, Giannatempo G, Pollice S, Maggialetti N, Carriero A, Di Costanzo A, Tedeschi G, Salvolini U. Role of advanced MR imaging modalities in diagnosing cerebral gliomas. La Radiol. Med. 2009; 114: 448–460.
7. Krabbe K, Gideon P, Wagn P, Hansen U, Thomsen C, Madsen F. MR diffusion imaging of human intracranial tumours. Neuroradiology 1997; 39: 483–489.
8. Sugahara T, Korogi Y, Kochi M, Ikushima I, Shigematu Y, Hirai T, Okuda T, Liang L, Ge Y, Komohara Y, Ushio Y, Takahashi M. Usefulness of diffusion-weighted MRI with echo-planar technique in the evaluation of cellularity in gliomas. J. Magn. Reson. Imaging 1999; 9: 53–60.
9. Kono K, Inoue Y, Nakayama K, Shakudo M, Morino M, Ohata K, Wakasa K, Yamada R. The role of diffusion-weighted imaging in patients with brain tumors. Am. J. Neuroradiol. 2001; 22: 1081–1088.
10. Yang D, Korogi Y, Sugahara T, Kitajima M, Shigematsu Y, Liang L, Ushio Y, Takahashi M. Cerebral gliomas: prospective comparison of multivoxel 2D chemical-shift imaging proton MR spectroscopy, echoplanar perfusion and diffusion-weighted MRI. Neuroradiology 2002; 44: 656–666.
11. Bulakbasi N, Guvenc I, Onguru O, Erdogan E, Tayfun C, Ucoz T. The added value of the apparent diffusion coefficient calculation to magnetic resonance imaging in the differentiation and grading of malignant brain tumors. J. Comput. Assisted Tomogr. 2004; 28: 735–746.
12. Seo HS, Chang K-H, Na DG, Kwon BJ, Lee DH. High b-value diffusion ($b = 3000\ s/mm^2$) MR imaging in cerebral gliomas at 3 T: visual and quantitative comparisons with $b = 1000\ s/mm^2$. Am. J. Neuroradiol. 2008; 29: 458–463.
13. Brunberg JA, Chenevert TL, McKeever PE, Ross DA, Junck LR, Muraszko KM, Dauser R, Pipe JG, Betley AT. In vivo MR determination of water diffusion coefficients and diffusion anisotropy: correlation with structural alteration in gliomas of the cerebral hemispheres. Am. J. Neuroradiol. 1995; 16: 361–371.
14. Lam WWM, Poon WS, Metreweli C. Diffusion MR imaging in glioma: does it have any role in the pre-operation determination of grading of glioma? Clin. Radiol. 2002; 57: 219–225.
15. Rollin N, Guyotat J, Streichenberger N, Honnorat J, Tran Minh V-A, Cotton F. Clinical relevance of diffusion and perfusion magnetic resonance imaging in assessing intra-axial brain tumors. Neuroradiology 2006; 48: 150–159.
16. Stadnik TW, Chaskis C, Michotte A, Shabana WM, van Rompaey K, Luypaert R, Budinsky L, Jellus V, Osteaux M. Diffusion-weighted MR imaging of intracerebral masses: comparison with conventional MR imaging and histologic findings. Am. J. Neuroradiol. 2001; 22: 969–976.
17. Higano S, Yun X, Kumabe T, Watanabe M. Malignant astrocytic tumors: clinical importance of apparent diffusion coefficient in prediction of grade and prognosis. Radiology 2006; 241: 839–846.
18. Murakami R, Hirai T, Sugahara T, Fukuoka H, Toya R, Nishimura S, Kitajima M, Okuda T, Nakamura H, Oya N, Kuratsu J, Yamashita Y. Grading astrocytic tumors by using apparent diffusion coefficient parameters: superiority of a one-versus two-parameter pilot method. Radiology 2009; 251: 838.
19. Tukey JW. *Exploratory Data Analysis*. Addison-Wesley Publishing Company: Reading, MA; 1977.
20. Emblem KE, Scheie D, Due-Tonnessen P, Nedregaard B, Nome T, Hald JK, Beiske K, Meling TR, Bjornerud A. Histogram analysis of MR imaging-derived cerebral blood volume maps: combined glioma grading and identification of low-grade oligodendroglial subtypes. Am. J. Neuroradiol. 2008; 29(9): 1664–1670.
21. Maes F, Collignon A, Vandermeulen D, Marchal G, Suetens P. Multimodality image registration by maximization of mutual information. IEEE Trans. Med. Imaging 1997; 16(2): 187–198.
22. Otsu N. A threshold selection method from gray-level histograms. IEEE Trans. Syst. Man Cybern. 1979; 9: 5.
23. Khayal IS, Polley M-YC, Jalbert L, Elkhaled A, Chang SM, Cha S, Butowski NA, Nelson SJ. Evaluation of diffusion parameters as early biomarkers of disease progression in glioblastoma multiforme. Neuro-Oncol. 2010; 12: 908–916.
24. Yin B, Liu L, Zhang BY, Li YX, Li Y, Geng DY. Correlating apparent diffusion coefficients with histopathologic findings on meningiomas. Eur. J. Radiol. 2012; 81(12): 4050–4056.
25. Nagar VA, Ye JR, Ng WH, Chan YH, Hui F, Lee CK, Lim CC. Diffusion-weighted MR imaging: diagnosing atypical or malignant meningiomas and detecting tumor dedifferentiation. Am. J. Neuroradiol. 2008; 29(6): 1147–1152.
26. Server A, Kulle B, Gadmar OB, Josefsen R, Kumar T, Nakstad PH. Measurements of diagnostic examination performance using quantitative apparent diffusion coefficient and proton MR spectroscopic imaging in the preoperative evaluation of tumor grade in cerebral gliomas. Eur. J. Radiol. 2011; 80(2): 462–470.
27. Arvinda HR, Kesavadas C, Sarma PS, Thomas B, Radhakrishnan VV, Gupta AK, Kapilamoorthy TR, Nair S. Glioma grading: sensitivity, specificity, positive and negative predictive values of diffusion and perfusion imaging. J. Neurooncol 2009; 94(1): 87–96.
28. Bode MK, Ruohonen J, Nieminen MT, Pyhtinen J. Potential of diffusion imaging in brain tumors: a review. Acta Radiol. 2006; 47(6): 585–594.
29. Hanley JA, McNeil BJ. A method of comparing the areas under receiver operating characteristic curves derived from the same cases. Radiology 1983; 148(3): 838–843.
30. Man MZ, Dyson G, Johnson K, Liao B. Evaluating methods for classifying expression data. J. Biopharm. Stat. 2004; 14(4): 1065–1084.
31. Zonari P, Baraldi P, Crisi G. Multimodal MRI in the characterization of glial neoplasms: the combined role of single-voxel MR spectroscopy, diffusion imaging and echo-planar perfusion imaging. Neuroradiology 2007; 49(10): 795–803.
32. Catalaa I, Henry R, Dillon WP, Graves EE, McKnight TR, Lu Y, Vigneron DB, Nelson SJ. Perfusion, diffusion and spectroscopy values in newly diagnosed cerebral gliomas. NMR Biomed. 2006; 19(4): 463–475.
33. Higano S, Yun X, Kumabe T, Watanabe M, Mugikura S, Umetsu A, Sato A, Yamada T, Takahashi S. Malignant astrocytic tumors: clinical importance of apparent diffusion coefficient in prediction of grade and prognosis. Radiology 2006; 241(3): 839–846.
34. Tien RD, Felsberg GJ, Friedman H, Brown M, MacFall J. MR imaging of high-grade cerebral gliomas: value of diffusion-weighted echoplanar pulse sequences. Am. J. Roentgenol. 1994; 162(3): 671–677.
35. Yang D, Korogi Y, Sugahara T, Kitajima M, Shigematsu Y, Liang L, Ushio Y, Takahashi M. Cerebral gliomas: prospective comparison of multivoxel 2D chemical-shift imaging proton MR spectroscopy, echoplanar perfusion and diffusion-weighted MRI. Neuroradiology 2002; 44(8): 656–666.
36. Kao HW, Chiang SW, Chung HW, Tsai FY, Chen CY. Advanced MR imaging of gliomas: an update. Biomed. Res. Int. 2013; 2013: 970586.
37. Kamel IR, Bluemke DA, Ramsey D, Abusedera M, Torbenson M, Eng J, Szarf G, Geschwind J-F. Role of diffusion-weighted imaging in estimating tumor necrosis after chemoembolization of hepatocellular carcinoma. Am. J. Roentgenol. 2003; 181: 708–710.
38. Chawla S, Kim S, Wang S, Poptani H. Diffusion-weighted imaging in head and neck cancers. Future Oncol. 2009; 5(7): 959–975.
39. Kim S, Loevner L, Quon H, Sherman E, Weinstein G, Kilger A, Poptani H. Diffusion-weighted magnetic resonance imaging for predicting and detecting early response to chemoradiation therapy of squamous cell carcinomas of the head and neck. Clin. Cancer Res. 2009; 15(3): 986–994.
40. Donati OF, Chong D, Nanz D, Boss A, Froehlich JM, Andres E, Seifert B, Thoeny HC. Diffusion-weighted MR imaging of upper abdominal organs: field strength and intervendor variability of apparent diffusion coefficients. Radiology 2014; 270(2): 454–463.
41. Koh DM, Collins DJ, Orton MR. Intravoxel incoherent motion in body diffusion-weighted MRI: reality and challenges. Am. J. Roentgenol. 2011; 196(6): 1351–1361.
42. Chandarana H, Kang SK, Wong S, Rusinek H, Zhang JL, Arizono S, Huang WC, Melamed J, Babb JS, Suan EF, Lee VS, Sigmund EE. Diffusion-weighted intravoxel incoherent motion imaging of renal tumors with histopathologic correlation. Invest. Radiol. 2012; 47(12): 688–696.
43. Federau C, Maeder P, O'Brien K, Browaeys P, Meuli R, Hagmann P. Quantitative measurement of brain perfusion with intravoxel incoherent motion MR imaging. Radiology 2012; 265(3): 874–881.
44. Federau C, Meuli R, O'Brien K, Maeder P, Hagmann P. Perfusion measurement in brain gliomas with intravoxel incoherent motion MRI. Am. J. Neuroradiol. 2014; 35(2): 256–262.
45. Bennett KM, Schmainda KM, Bennett RT, Rowe DB, Lu H, Hyde JS. Characterization of continuously distributed cortical water diffusion rates with a stretched-exponential model. Magn. Reson. Med. 2003; 50(4): 727–734.